# New Radical Detected by HF-EPR, ENDOR, and Pulsed EPR in a Room Temperature Irradiated Single Crystal of Glycine

**Marina Brustolon,* Vasile Chis,† and Anna Lisa Maniero**

*Dipartimento di Chimica Fisica, Via Loredan 2, I-35131, Padova, Italy*

**Louis-Claude Brunel**

*National High Magnetic Field Laboratory, 1800 East P. Dirac Drive, Tallahassee, Florida 32310*

*Received: January 28, 1997; In Final Form: April 25, 1997*[⊗]

Single crystals of room temperature $\gamma$-irradiated glycine have been studied with electron nuclear double resonance (ENDOR) and X-band and high-frequency continuous wave electron paramagnetic resonance (EPR) spectroscopies and electron spin echo spectroscopy. EchoEPR spectroscopy was used to distinguish the radicals with different phase memory relaxation times. Three radicals have been detected, which have been identified as $NH_3^+-CH-COO^-$ (radical A), $CH_2-COO^-$ (radical B), and $CH_2-NH_2$ (radical C). Whereas radicals A and B had been observed by other authors in the past, radical C was not detected previously. The hyperfine tensors of the two $CH_2$ protons and of one of the $NH_2$ protons were determined by ENDOR. ESEEM (electron spin echo envelope modulation) and HYSCORE (hyperfine sublevel correlation spectroscopy) experiments were performed in order to obtain the relative signs of the hyperfine coupling constants of the three protons. The principal values and the principal directions of the hyperfine tensors are in agreement with the hypothesis of a nonplanar structure of the radical. Unrestricted Hartree−Fock calculations have been carried out for different conformations of radical C. The calculated hyperfine coupling constants are compared with the experimental results.

## Introduction

The different radicals produced by high-energy irradiation of solid glycine have been the subject of many studies since the beginning of the EPR spectroscopy age.[1]

This aminoacid, in spite of its semplicity, gives rise under irradiation to a large variety of different radicals. Low-temperature irradiation studies have shown that the anion and cation radicals formed initially evolve along a series of thermally unstable radicals.[2,3] The rates of the reactions are strongly temperature dependent, and therefore the nature of the observed radicals depends on the temperature of irradiation and on the thermal history of the irradiated crystal.

The cw-EPR (continuous wave EPR) spectrum of room temperature X- or $\gamma$-irradiated glycine crystals has been attributed to the superposition of the spectra of two radicals:[1] $NH_3^+-CH-COO^-$ (radical A), $CH_2-COO^-$ (radical B). These radicals are formed from the primary anion and cation radicals respectively for deprotonation and deamination.[4]

The hyperfine coupling tensors of radical A have been determined from the room temperature EPR spectra of a glycine crystal irradiated at 77 K, since in this case radical A is the more stable radical at room temperature.[1] The hyperfine coupling tensors of the two protons of radical B have been determined by an ENDOR study at low temperature.[5] At room temperature the two protons are equivalent, since the methylene is rotating fastly.[1]

A third type of radical usually formed in irradiated aminoacids is produced by decarboxylation of the primary anion radical. This type of radical was never observed in the past in room temperature irradiated glycine.

However, in the previous EPR studies no conclusive evidence had been reached that the latter radicals were the only ones stable at room temperature. In fact, the cw-EPR spectra of this system is particularly difficult to interpret, for the following reasons. First of all, many satellite forbidden lines due to the simultaneous flip of the electron spin and of a weakly coupled proton are present. Since the relative intensities of the forbidden and allowed EPR lines depend on the microwave power, the spectral profile is also strongly dependent on it. Moreover, for radical B an incomplete averaging of the hyperfine tensors anisotropies of the methylene protons at room temperature is to be expected on the basis of the high-energy barrier hindering the $CH_2$ rotation, measured for the same radical in other systems.[6] Therefore the intensities and widths of the EPR lines of the latter radical are expected to depend on the orientation of the crystal in the magnetic field.

To determine the radicals stable at room temperature, we decided to carry out a complete ENDOR study on $\gamma$-irradiated glycine crystals.

In addition to the latter study we used several advanced EPR techniques in order to interpret unambigously the ENDOR results. We performed a series of experiments based on electron spin echoes, in particular EchoEPR (EEPR), ESEEM, and the two-dimensional spin echo modulation experiment HYSCORE.[7] High-field EPR (HF-EPR) experiments have been also performed, since this technique is of paramount importance to get a good insight in the systems where more than one type of radical is formed.

## Experimental Section

Single crystals of glycine were obtained by slow evaporation at room temperature of a water solution. Glycine crystallizes in the monoclinic space group $P2_1/c$, with cell parameters $a$ = 5.1054, $b$ = 11.9688, $c$ = 5.4645 Å, $\beta$ = 111.7°, and $Z$ = 4.[8] The crystals were irradiated at room temperature by $\gamma$-rays from a $^{60}Co$ source with a dose of 3 Mrad. Two types of irradiated single crystals have been studied: i. freshly irradiated ones (after some days), ii. aged after irradiation (after some months).

† Present address: Babes Bolyai University, Dept. of Physics, 1, Kogalniceanu, RO-3400 Cluj-Napoca, Romania.

[⊗] Abstract published in *Advance ACS Abstracts,* June 15, 1997.

S1089-5639(97)00347-2 CCC: $14.00 

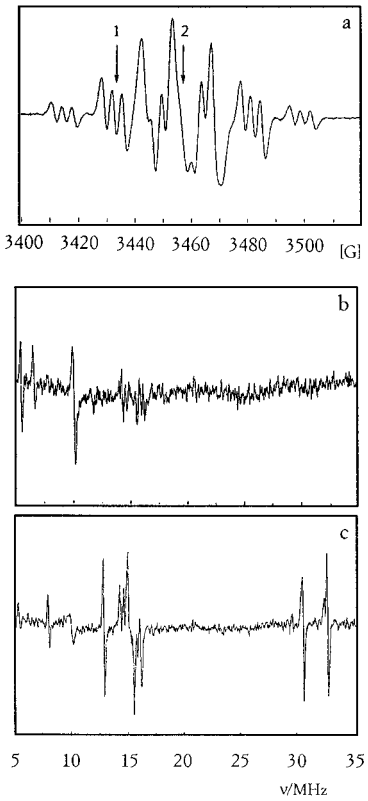


**Figure 1.** a. X-band cw-EPR spectrum of a single crystal of glycine a week after irradiation ($T$ = 290 K, $B||c$). b. ENDOR spectrum obtained on position 1 in the EPR spectrum. c. ENDOR spectrum obtained on position 2 in the EPR spectrum.

ENDOR spectra were recorded at the temperature of 280 K in the three crystallographic planes every 6°. For this purpose, a single crystal was mounted on a goniometer rod and rotated in the EPR cavity around the three crystal axes *abc*.

ENDOR spectra were obtained by using a Bruker ER200 D spectrometer with a Bruker $TM_{110}$ cavity containing a radio-frequency (rf) coil. The rf is generated by a Rohde&Schwarz SMX synthesizer and swept in the proton frequency range by a computer that also provides for the data acquisition. The rf is frequency modulated with 25 kHz by using a EG&G 5208 lock-in, and the ENDOR signal is recorded as the first derivative. Amplification of the FM modulated rf is achieved with an ENI A-300 amplifier.

The pulsed experiments were performed by using a Bruker ESP 380 spectrometer equipped with a dielectric Bruker cavity. The nature of the experiments and the values of the parameters used will be discussed later.

HF-EPR spectra were recorded at the high-field electron magnetic resonance facility of the National High Magnetic Field Laboratory in Tallhassee, Florida. The EPR spectrometer is of similar design to the instrument described by Mueller et al.,[9] except for the following modifications: the sources are Gunn diodes oscillators (from ABmm, Paris), equipped with Schottky diode harmonic generators; the magnetic field is provided by a 15/17 T (at 4.2 and 2.2 K, respectively) superconducting Oxford Instruments magnet, and the detector is a "hot electron" InSb bolometer (from QMC, London). The spectra are recorded in the magnetic field first derivative mode.

## Results

**X-band cw-EPR.** Due to the monoclinic crystal structure of glycine, two magnetically non equivalent sites are present. Therefore, for any orientation of the crystal in the magnetic field, the spectrum is given by the superposition of the spectra due to the radicals in the two sites.

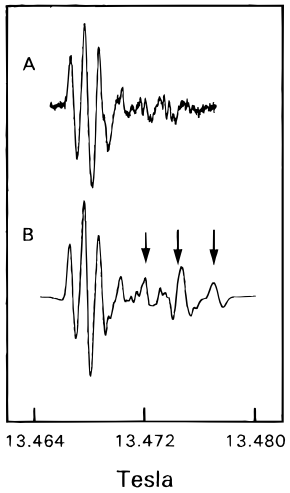


**Figure 2.** High-field EPR spectra with $B||c$ ($T$ = 290 K). Microwave frequency 375 GHz: *a*. an aged glycine irradiated crystal, and *b*. a freshly irradiated one. The arrows indicate the EPR lines attributed to radical *B*.

However, when the magnetic field is along a crystallographic axis, or when it is in the crystallographic plane perpendicular to the *b* axis, the two sites become magnetically equivalent. The pronounced asymmetry of the spectra also for these latter orientations indicates the superposition of spectra due to different radicals. In Figure 1a the X-band EPR spectrum for $B||c$ is reported.

The outer lines of the spectrum show the triplet due to the hyperfine coupling with the $^{14}N$, and belong to the well-characterized radical A. Slight differences can be noted in the spectra as the crystals age after irradiation.

Due to the complexity of the spectra, we did not try a full analysis by rotating the crystal around the three crystallographic axes.

**HF-EPR.** The HF-EPR for a freshly irradiated and an aged crystals for $B||c$ are shown in Figure 2.

In the aged crystals two radicals are present, radical A and one giving rise to the low-field triplet, whereas in the freshly irradiated one a third radical can be detected, as indicated by the arrows. The hyperfine splitting of the low-field triplet is about 11 G, whereas that of the triplet indicated by the arrows is of 21 G. Therefore this latter triplet can be attributed to radical B. On the other hand, the low-field triplet is due to a radical not detected before.

The $g$ values for the three radicals are radical A, $g = 2.003\,94 \pm 0.000\,02$; radical B, $g = 2.003\,45 \pm 0.000\,02$; low-field triplet $g = 2.004\,48 \pm 0.000\,02$. It should be noted that the $g$ value for radical B with $B||c$ was measured many years ago by Box et al. They found $g = 2.0038$.[2]

**ENDOR.** The ENDOR investigation has been done in the frequency interval 5−35 MHz. In this frequency range the ENDOR spectra of the aged and freshly irradiated crystals are the same.

We will consider in the following only proton ENDOR transitions. We will call high-frequency ENDOR transitions $\nu_+$ those given by $\nu_+ = |A/2| + \nu_H$, where $A$ is approximately the hyperfine splitting and $\nu_H$ the free proton frequency, and low-frequency ENDOR transitions $\nu_-$ are the ones given by $\nu_- = ||A/2| - \nu_H|$. To attribute an ENDOR line to a $\nu_+$ or $\nu_-$ frequency, we observed its radiofrequency shift corresponding to different values of the fixed external magnetic field.

Depending on the positive or negative sign of the hyperfine coupling, the lines at frequency ($\nu_+$, $\nu_-$) will correspond respectively to the ($m_s = -1/2$, $m_s = +1/2$) or to the ($m_s = +1/2$, $m_s = -1/2$) electron spin manifolds.

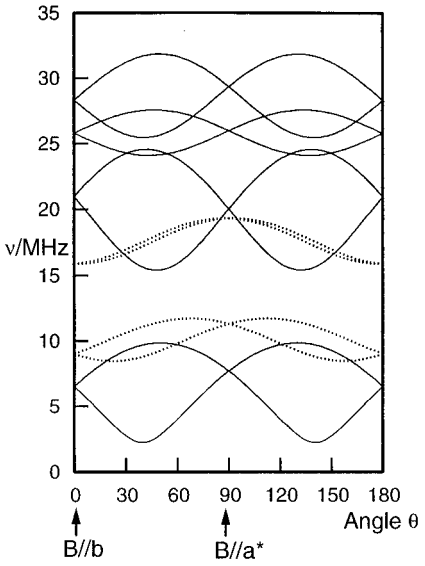


**Figure 3.** Angular dependences of the ENDOR frequencies with the magnetic field exploring the *a***b* crystallographic plane ($T = 280$ K). The dotted lines are the angular dependences of the $\nu_-$ frequencies of the α-proton (upper curves) and of the $NH_3$ protons (lower curves) of radical *A*. The three upper pairs of curves with continuous line are the $\nu_+$ frequencies of protons *1*, *2*, and *3* of radical *C* (see Table 2); the lower pair of curves are the $\nu_-$ frequencies of proton *2*.

**TABLE 1: Hyperfine Tensors of the Protons of $NH_3$ Group in Radical A**[a]

| isotropic coupling (MHz) | dipolar tensor principal values (MHz) | direction cosines | | |
|---|---|---|---|---|
| | | *a** | *b* | *c* |
| | 5.4 | 0.8113 | 0.3202 | −0.4889 |
| 48.8 | −3.1 | 0.5638 | −0.6490 | 0.5106 |
| | −2.3 | −0.1538 | −0.6900 | −0.7072 |

[a] Only one magnetically inequivalent site is reported.

The measured ENDOR frequencies for any orientation of the crystal in the magnetic field depend upon the irradiated EPR hyperfine component. In Figure 1 the EPR spectrum for the magnetic field aligned with the *c* crystallographic axis is shown (Figure 1a), together with the ENDOR spectra observed on the different hyperfine lines (Figure 1b,c).

The ENDOR transitions observed on the outer components of the EPR spectrum are due to radical A. By comparing the angular dependence of the ENDOR lines with that calculated on the basis of the hyperfine tensors reported in ref 1, we were able to attribute the frequencies observed to the three equivalent $NH_3$ protons, to the α-proton, and to the N nucleus. We followed the angular dependence of the ENDOR lines due to the α-proton in the ab plane (Figure 3), but in the other planes the intensities of the latter lines were very weak, and we did not try to obtain the hyperfine tensor from the ENDOR data. On the other hand, we were able to follow in the three planes the ENDOR frequencies due to the three equivalent protons of the rotating $NH_3$ group. From the usual first-order analysis of the angular dependences of these frequencies we have obtained the hyperfine tensors reported in Table 1. This tensor is very similar to the one obtained by EPR spectroscopy.

When the magnetic field is set on the central EPR lines, other ENDOR lines appear both at lower and higher frequencies with respect to the free nucleus frequency $\nu_H$, as expected on the basis of the hypothesis of the presence of other radicals besides radical A.

The angular dependences of the ENDOR lines observed in the 5−35 MHz range on rotating the crystal around *c* are shown in Figure 3. Both the proton ENDOR frequencies $\nu_-$ belonging to the radical A and the frequencies belonging to the unknown radical(s) are shown. At frequencies higher than 35 MHz, only the partner ENDOR lines $\nu_+$ of the α-proton and of the $NH_3$ protons of radical A were detected.

The crystal was rotated around the three crystallographic axes, and by the usual first-order analysis of the angular dependences of the frequencies of the lines corresponding to the unknown radical(s) three pairs of hyperfine tensors were obtained, reported in Table 2.

Many other ENDOR lines in the vicinity of $\nu_H$ were observed; we did not try to analyze them. Moreover, a complicated pattern of lines was also present al low frequency, and we attributed them to the $^{14}N$ nuclei present in the radical(s). Also these lines have not been analyzed.

**ECHOEPR.** Pulsed EPR spectroscopy in solids allows the detection of electron spin echoes. The amplitude of the electron spin echo depends on the number of spin packets involved in the echo formation and on the rate of their stochastic relaxation processes. The characteristic time of decay of the echo intensity on increasing the time interval between the two pulses is called phase memory time $T_M$.

The EchoEPR (EEPR) spectra are obtained by recording the two pulses Hahn echo amplitude as a function of the magnetic field.[10] When the relaxation rate $T_M$ is the same for all the spin packets, the EEPR and the EPR spectra give the same information. On the other hand, if more than one type of radical is present, and the different radicals have different $T_M$s, the two types of spectra can be substantially different. In fact in the latter case in the EEPR spectrum the intensity of the lines due to the different radicals are different. Moreover, the EEPR spectrum profile depends on the time interval between the two pulses.

In Figure 4 we report the integrated form of the cw-EPR spectrum for $B||c$ (Figure 4a), the EEPR spectrum for the same orientation (Figure 4b), and their difference (Figure 4c). The latter spectrum is evidently due to the same species giving rise to the low-field triplet in the HF-EPR spectrum (see Figure 2). The EEPR spectrum does not show the presence of this latter radical, due to its phase memory time $T_M$, much shorter than that of radical A.

**ESEEM and HYSCORE.** The electron spin echo envelope modulation (ESEEM) allows to measure the nuclear transitions frequencies in solids with anisotropic hyperfine interactions.[11] Therefore in our case this experiment gives the same information as that of the ENDOR spectra. However, in order to perform a two-dimensional HYSCORE experiment, an ESEEM study is necessary, allowing a correct orientation of the crystal in the magnetic field and a suitable choice for the pulse lenghts and time intervals duration.

We have performed an ESEEM analysis only in the *ab* plane. The pulse sequence

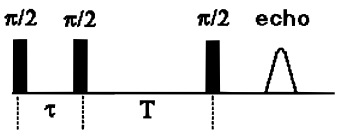


has been used, giving rise to the so-called stimulated echo.

For an electron coupled with a nucleus giving rise to ENDOR frequencies $\nu_+$ and $\nu_-$, the stimulated echo modulation corresponding to the two frequencies is given by the expression[12]

$$E_{mod} = 1 - \frac{K}{4}[(1 - \cos(2\pi\nu_+\tau))(1 - \cos(2\pi\nu_-\tau')) + (1 - \cos(2\pi\nu_-\tau))(1 - \cos(2\pi\nu_+\tau'))]$$

where $\tau' = \tau + T$. In order to avoid the "blind spots", i.e., the values of $\tau$ such that $\nu_i\tau = n$, where $n$ is an integer, we have

**TABLE 2: Hyperfine Tensors of the Protons of Radical C[a]**

| | isotropic coupling (MHz) | dipolar tensor principal values (MHz) | direction cosines | | |
|---|---|---|---|---|---|
| | | | *a** | *b* | *c* |
| | | 15.7 | 0.0684 | 0.0466 | 0.9965 |
| proton 1 | −20.2 | −14.7 | 0.7433 | 0.6638 | −0.0821 |
| | | −1.0 | −0.6654 | 0.7464 | 0.0107 |
| | | 14.4 | 0.738 | −0.5961 | 0.3162 |
| proton 2 | −18.8 | −13.4 | 0.319 | −0.1046 | −0.9419 |
| | | 1.0 | −0.5945 | −0.796 | −0.1129 |
| | | 17.3 | 0.4693 | −0.3809 | −0.7966 |
| proton 3 | 25.0 | −11.6 | 0.7509 | −0.3024 | 0.5870 |
| | | −5.7 | −0.4645 | −0.8737 | 0.1441 |

[a] Only one magnetically inequivalent site is reported.

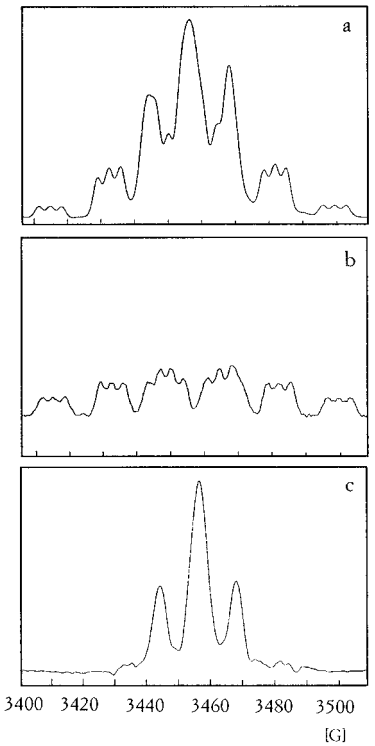


**Figure 4.** *a.* Integrated cw-EPR spectrum for a freshly irradiated single crystal of glycine ($B||c$, $T = 290$ K). *b.* EEPR spectrum for the same crystal at the same orientation (Hahn echo, pulse duration 80 ns, time interval between pulses 240 ns). *c.* Difference between spectra *a* and *b.*

collected for each orientation of the crystal in the magnetic field a series of 10 echo decays corresponding to 10 different values of $\tau$. $K$ is the so-called modulation depth.

The angular dependences of the ESEEM frequencies in the $a^*b$ plane have been compared with the ENDOR ones reported in Figure 3. The angular dependences of the $\nu_+$ frequencies belonging to protons 1, 2, and 3 can be followed, and they are in very good agreement with the ENDOR results, as expected.

We performed an HYSCORE (hyperfine sublevel correlation spectroscopy) experiment with $B||a^*$. This is a four-pulse experiment that can be considered as derived from the three-pulse experiment described above by inserting a $\pi$ pulse between the second and third $\pi/2$ pulses.[7]

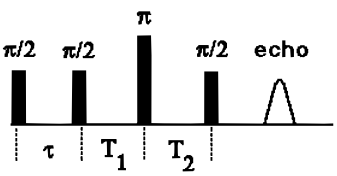


The stimulated echo is recorded for different values of $T_1$ and $T_2$. A Fourier transform with respect to $T_1$ and $T_2$ gives rise to a two-dimensional spectrum, with diagonal peaks corresponding to the nuclear frequencies and off diagonal cross-peaks connecting only nuclear transitions belonging to the same radical. Moreover, the theoretical analysis of this experiment shows that the correlation peaks between two nuclear transitions belonging to two different nuclei are present only if the the two transitions belong to the two different $m_s = 1/2$ and $m_s = -1/2$ manifolds.[13]

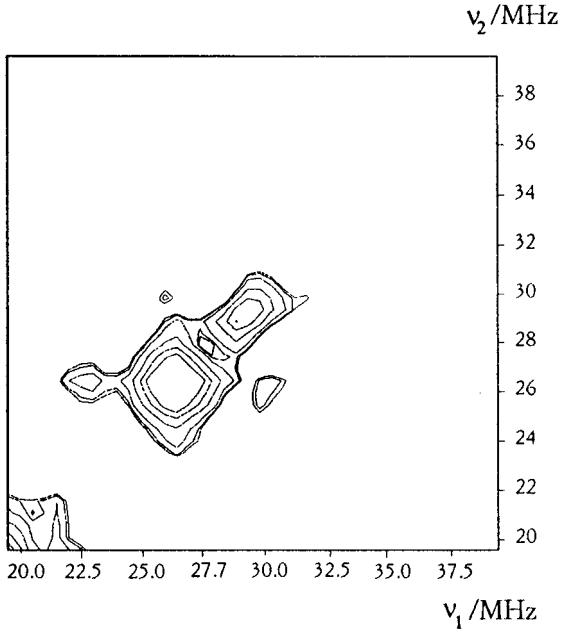


**Figure 5.** Contour plot of the FT-Hyscore spectrum in the region 20−32 MHz ($B||a^*$) at $T = 290$ K. Pulse widths 16 ns for $\pi/2$ pulses and 32 ns for $\pi$, time interval between the two $\pi/2$ pulses 160 ns. The magnetic field B was positioned on the center of the EPR spectrum. The two coalescing diagonal peaks correspond to the $\nu_+$ frequencies of protons *1* and *2* (26 and 30 MHz). The two weak cross peaks indicate that the two ENDOR transitions belong to different $m_s$ manifolds, and therefore the two hyperfine tensors elements for $B||a^*$ must have opposite sign (see text).

Therefore a correlation peak between two $\nu_{+1}$ and $\nu_{+2}$ frequencies, where 1 and 2 indicate two different nuclei, indicates that the two corresponding hyperfine couplings have opposite signs.

As shown in Figure 5, weak correlation peaks are present between the $\nu_+$ frequencies of protons 1 and 3. We can therefore conclude that the two corresponding hyperfine couplings for $B||a^*$ have different signs.

## Discussion

The HF-EPR spectrum for $B||c$ of the freshly irradiated crystal (Figure 2) is due to the superposition of the spectra of three different radicals. Besides the well-characterized spectrum of radical A, the triplet indicated by the arrows can be attributed to radical B on the basis of its hyperfine splitting (21 G), whereas the low-field triplet, with a hyperfine splitting of about 11 G must be attributed to another radical not observed previously, let us call it radical C. The difference between the EPR and EEPR spectra for $B||c$ shows the same triplet attributed to radical C. As discussed below, this spectrum has been simulated (see Figure 6) by assuming that the three hyperfine tensors obtained from the ENDOR analysis and reported in Table 2 are due to the latter radical, each tensor corresponding to a single proton.

Since the HF-EPR spectrum of the aged crystal does not show the presence of radical B, we must conclude that radicals A and C are more stable than B.

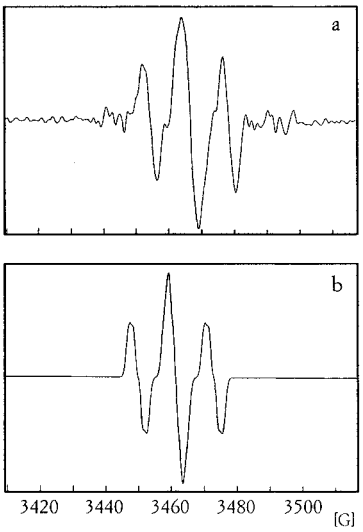


**Figure 6.** *a*. Spectrum reported in Figure 4*c*, in derivative form. *b*. Simulation of the same spectrum as due to radical *C* for $B||c$. The spectrum has been simulated with $A_{H1} = 12.1$ G, $A_{H2} = 10.8$ G, $A_{H3} = 1.4$ G, and $A_N = 1.5$ G. The splitting constants for the three protons have been obtained from the ENDOR tensors in Table 2.

Let us now discuss the nature of radical C. The principal values of hyperfine tensors 1 and 2 in Table 2 are very similar. The antiaxiality of the dipolar principal values is typical of those of α-protons. However, both their dipolar values and isotropic hcc's are smaller than those for an α-proton bonded to a carbon atom with spin density $\rho = 1$ in a $\pi$-radical (about −30, −60, and −90 MHz). The small values of the isotropic hyperfine constants can be explained either by a spin delocalization on a conjugated $\pi$-system, or by a partial $\sigma$-character of the orbital bearing the unpaired electron. The small principal values of the dipolar tensor can be explained also by a spin delocalization on a conjugated $\pi$-system, or by large amplitude vibrations of the C−H bonds.[14]

The hyperfine tensor 3 is different from the previous ones. By assuming that, as usual, the largest principal value of the dipolar tensor is positive, a positive hcc is obtained from the trace of the tensor.

The HYSCORE experiment shows that the sign of the hyperfine couplings of protons 1 and 3 for $B||a^*$ are different. From this result we obtain a negative sign for the hcc's of protons 1 and 2.

To have some insight into the structure of the radical, we compared the principal directions of the hyperfine tensors with the atomic intramolecular directions in the undamaged crystal, as obtained from the crystal structure.

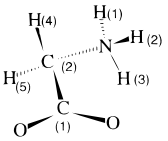


For the hyperfine tensor 1 the principal direction corresponding to the principal value +15.7 MHz coincides with an approximation of 7° with the C(1)−C(2) bond in the undamaged molecule. On the other hand, the principal direction corresponding to the principal value +14.4 MHz for proton 2 coincides with an approximation of 6° with the line bisecting the angle H(4)−C(2)−H(5).

For an α-proton, the principal value of the dipolar tensor with a positive sign corresponds to the C−H bond direction.[14] The latter results indicate that the two α-protons 1 and 2 belong to the glycine $CH_2$ group. Therefore radical C must derive from a decarboxylation of the glycine molecule, since the radicals obtained by deamination have been already characterized.

It should be noted that Bonazzola et al.[15] in an EPR study on a single crystal of glycine irradiated at 77 K and then UV photolyzed detected the presence of the radical $CH_2-NH_3^+$. The hyperfine tensors obtained in that study are however different from those obtained in the present work. A trivial candidate for radical C is therefore $CH_2-NH_2$.

As explained above, we simulated the spectrum of radical C obtained as the difference between the EPR and the EEPR spectra for $B||c$ (Figure 6). We assumed that only one proton corresponds to each of the hyperfine tensors 1, 2, and 3 reported in Table 2. A better agreement between the experimental and simulated spectra was obtained considering a small hyperfine coupling (1.5 G) with a $^{14}N$ nucleus. We did not try to get a still better agreement by changing the simulation parameters, since the shapes and intensities of the EPR lines of the difference spectrum itself depend on the parameters of the EEPR and on the difference procedure.

We assign the hyperfine tensor 3 to a proton bonded to the N atom. This attribution is confirmed by the following considerations. On the basis of the comparison, reported above, between the bond directions in the undamaged molecule and the principal directions of the hyperfine tensors of protons 1 and 2, when radical C is formed the C(2)H(4)H(5) group rearranges itself in a way that can be described by two rotations in sequence. The first one is a rotation of 120° around the C(2)−N bond, so that the C(2)−H(4) bond is now aligned with the direction of the former C(2)−C(1) bond. The second one is a rotation of 60° around the new C(2)−H(4) bond, so that the C(2)−H(5) bond is now lying along the line bisecting the angle between the two original C−H directions. The latter rotation also rotates the C(2)−N bond.

The $NH_3$ group is fastly rotating as far as the room temperature EPR and ENDOR spectra are considered. However, the coordinates of the minima of the three wells of the potential energy for the three $NH_3$ protons are determined by the neutron diffraction study.[8] By assuming that the rotation considered above rotates rigidly the C(2)−NH(1)H(2)H(3) group, we are able to calculate the new positions of the three protons of the $NH_3$ group. The principal direction corresponding to the largest principal value of the dipolar tensor of proton 3 agrees well with the C(2)···H(1) direction calculated for H(1) in this rotated position. Moreover, we can compare the largest principal value of the dipolar tensor of proton 3 with the one calculated for the interaction between the unpaired electron localized on the carbon atom with the H(1) proton, on the basis of the point dipole approximation.[14]

By assuming that the C(2)···H(1) distance in the radical is the same as in the crystal structure, one obtains a value of 17 MHz, in very good agreement with the experimental one.

Therefore we can conclude that radical C is most probably a radical $CH_2-NH_2$, in which one of the two protons of the $NH_2$ group has a small hyperfine tensor.

The unusual values of the hyperfine tensors of protons 1 and 2 can be compared with those obtained by Bonazzola et al. for the radical $CH_2-NH_3^+$.[15] The dipolar coupling tensors for the two α-protons in the latter radical (respectively +13.1, 0.3, −13.4 MHz and +12.9, −0.3, and −12.6 MHz) are very similar to those obtained in the present work. On the other hand, for the radical above the isotropic hcc's are respectively −42.5 and −45.1 MHz, about the double than in our case. The latter radical is supposed to be nonplanar on the basis of the comparison between the experimental and calculated hyperfine couplings. However, it should be noted that the angle between the two principal directions corresponding to the two C−H

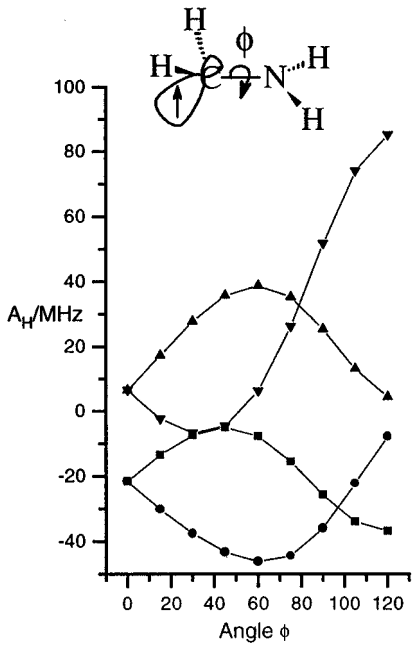


**Figure 7.** Calculated hyperfine coupling constants (UHF method) for the $CH_2NH_2$ radical on assuming a tetrahedral arrangement of the C−H and N−H bonds.The bond lenghts were assumed to be the same as in the undamaged molecule: C−N 1.47 Å, C−H 1.09 Å, N−H 1.05 Å. The angle $\phi$ is defined in the box; $\phi = 0$ corresponds to a staggered conformation: Triangles, $NH_2$ protons; Squares and circles, $CH_2$ protons.

directions of the dipolar tensors of the $CH_2$ protons determined in the latter study is of 117°.

In our case the corresponding angle has a value of 109°, indicating that the unpaired electron in the radical is in a nearly $sp^3$ orbital. We can therefore conclude that the two compared radicals must have a similar mobility for the C−H bonds, but a different degree of bending outside from the planar conformation.

We perfomed unrestricted Hartree−Fock calculations on the radical $CH_2-NH_2$ with the aim of comparing the values of the isotropic hcc's of the $CH_2$ and $NH_2$ protons with the experimental ones for different conformations of the radical. It should be noted that the structure of the $CH_2-NH_2$ radical in an isotropic medium has been recently calculated by Armstrong et al. by using ab initio calculations.[16] They find that the radical is pyramidal at both N and C, with a staggered arrangement of the C−H and N−H bonds.

For our calculations of the radical in an anisotropic matrix we did not perform a structure optimization, and we used the bond lenghts and angles obtained from the crystal structure for the undamaged molecule and reported in the caption of Figure 7. The energy was minimized at an UHF-SCF level, by using the semiempirical AM1 hamiltonian, as implemented in the MOPAC version 6.0 package.[17] The spin contamination is very small, since $\langle S^2 \rangle = 0.754$, and therefore no quartet annihilation was performed.

A number of calculations were carried out on varying the angle $\phi$ defined in the box of Figure 7. The results are reported in the same figure. The hcc's of the two protons of the $CH_2$ group are always smaller than the hcc of an α-proton for an aliphatic $\pi$ radical CHRR′ (about −60 MHz). Moreover, the calculated hyperfine couplings of the four protons depend on the conformation of the radical. In particular, for some values of the angle $\phi$, the calculated hcc's of the two protons of the $NH_2$ group are very different, since one of the two hcc's becomes very small. This result is in agreement with the experimental finding that only one proton of the latter group has an appreciable hcc.

We did not try a closer comparison between the calculated and experimental values. In fact to obtain reliable calculated hyperfine tensors one should calculate first of all the equilibrium structure of the radical in the crystal matrix. Since the geometry of the radical is expected to be strongly determined by the H-bonds with the neighbour molecules, the orientation of the radical in the matrix should also be determined precisely by comparing the calculated dipolar part of the hyperfine tensors with the experimental ones.

An extensive ab initio calculation will be performed in the future for this aim.

## Conclusions

In room temperature $\gamma$-irradiated glycine crystals, three different radicals are formed, $NH_3^+-CH-COO^-$ (radical A), $CH_2-COO^-$ (radical B), and $CH_2-NH_2$ (radical C).

Radicals A and C are stable for months, whereas radical B decays in some weeks.

Radical C is due to the decarboxylation of the primary radical anion, and it was not detected previously. Three proton hyperfine tensors have been determined for this radical, corresponding to the two α-protons and to one of the $\beta$-protons, whereas the hyperfine tensors of the other $\beta$-proton and of the $^{14}N$ are too small to be detected in the EPR spectra.

From the principal directions of the hyperfine tensors corresponding to the $C-H_1$ and $C-H_2$ bond directions forming an angle of 109° and from the small value of the isotropic hcc's one deduces that the latter radical is not planar.

The small values of the dipolar coupling tensors elements of the α-protons indicate large amplitude librations of the C−H bonds. These motions modulate the hyperfine tensors, and they constitute therefore a powerful relaxation mechanism. The latter one is probably responsible of the relaxation behavior of the radical, which at room temperature has a phase memory time much shorter than that of radical A, as shown by the difference between cw-EPR and echo-detected EPR.

**Acknowledgment.** We thank Prof. M. Gabriella Severin, Dipartimento di Chimica Fisica, Padova, Italy, for her valuable help in the calculations and Dr. Pier Giorgio Fuochi, F. R.A. E., Bologna, Italy, for the irradiation of the samples. This work has been in part supported by the Centro di Studio sugli Stati Molecolari Radicalici ed Eccitati, C. N. R., Padova, Italy.

## References and Notes

(1) Morton, J. R. *J. Am. Chem. Soc.* **1964**, *86*, 2325 and references cited therein.
(2) Box, H. C.; Freund, H. G.; Budzinski, E. E. *J. Am. Chem. Soc.* **1966**, *88*, 658.
(3) (a) Sinclair, J. *J. Chem Phys.* **1971**, *55*, 245. (b) Muto, H.; Iwasaki, M.; Takahashi, Y. *J. Chem. Phys.*, **1977**, *66*, 1943.
(4) Box, H. C. *Radiation Effects: ESR and ENDOR Analysis*; Academic Press: New York, 1977.
(5) Teslenko, V. V.; Gromovoi, Yu.S.; Krivenko, V. G. *Mol. Phys.* **1975**, *30*, 425.
(6) Brustolon, M.; Maniero, A. L.; Segre, U. *Mol. Phys*. **1988**, *65*, 447.
(7) Höfer, P.; Grupp, A.; Nebenführ, H.; Mehring, M. *Chem. Phys. Lett.* **1986**, *132*, 279.
(8) Jönsson, P.-G.; Kvick, Å. *Acta Crystallogr*. **1971**, *B28*, 1827.
(9) Mueller, F.; Hopkins, M. A.; Coron, N.; Grynberg, M.; Brunel, L. C; Martinez, G. *Rev. Sci. Instrum.*, **1989**, *60*, 3681.
(10) Millhauser, G. L., Freed, J. H. *J. Chem. Phys.* **1984**, *81*, 37.
(11) Mims, W. B. *Phys. Rev. B* **1972**, *5*, 2409.
(12) Schweiger, A. In *Modern Pulsed and Continuous-Wave Electron Spin Resonance*; Kevan, L., Bowman, M. K., Eds.; Wiley: New York, 1990.
(13) Gemperle, C.; Aebli, G.; Schweiger, A.; Ernst, R. R. *J. Magn. Reson.* **1990**, *88*, 241.
(14) Atherton, N. M. *Principles of Electron Spin Resonance*; Ellis Horwood and Prentice Hall: New York, 1993.
(15) Bonazzola, L.; Iacona, C.; Michaut, J. P.; Roncin, J. *J. Chem. Phys.* **1980**, *73*, 4175.
(16) Armstrong, D. A.; Rauk, A.; Yu, D. *J. Am. Chem. Soc.* **1993**, *115*, 666.
(17) Stewart, J. J. QCPE Program, Version 455.